

Low-frequency electrical response to microbial induced sulfide precipitation

Dimitrios Ntarlagiannis,¹ Kenneth Hurst Williams,^{2,3} Lee Slater,¹ and Susan Hubbard²

Received 17 February 2005; revised 9 July 2005; accepted 12 September 2005; published 19 November 2005.

[1] We investigated the sensitivity of low-frequency electrical measurements to microbe-induced metal sulfide precipitation. Three identical sand-packed monitoring columns were used; a geochemical column, an electrical column and a control column. In the first experiment, continuous upward flow of nutrients and metals in solution was established in each column. Cells of *Desulfovibrio vulgaris* (*D. vulgaris*) were injected into the center of the geochemical and electrical columns. Geochemical sampling and post-experiment destructive analysis showed that microbial induced sulfate reduction led to metal precipitation on bacteria cells, forming motile biominerals. Precipitation initially occurred in the injection zone, followed by chemotactic migration of *D. vulgaris* and ultimate accumulation around the nutrient source at the column base. Results from this experiment conducted with metals show (1) polarization anomalies, up to 14 mrad, develop at the bacteria injection and final accumulation areas, (2) the onset of polarization increase occurs concurrently with the onset of lactate consumption, (3) polarization profiles are similar to calculated profiles of the rate of lactate consumption, and (4) temporal changes in polarization and conduction correlate with a geometrical rearrangement of metal-coated bacterial cells. In a second experiment, the same biogeochemical conditions were established except that no metals were added to the flow solution. Polarization anomalies were absent when the experiment was replicated without metals in solution. We therefore attribute the polarization increase observed in the first experiment to a metal-fluid interfacial mechanism that develops as metal sulfides precipitate onto microbial cells and form biominerals. Temporal changes in polarization and conductivity reflect changes in (1) the amount of metal-fluid interfacial area, and (2) the amount of electronic conduction resulting from microbial growth, chemotactic movement and final coagulation. This polarization is correlated with the rate of microbial activity inferred from the lactate concentration gradient, probably via a common total metal surface area effect.

Citation: Ntarlagiannis, D., K. H. Williams, L. Slater, and S. Hubbard (2005), Low-frequency electrical response to microbial induced sulfide precipitation, *J. Geophys. Res.*, 110, G02009, doi:10.1029/2005JG000024.

1. Introduction

[2] In anoxic environments and under low temperatures (i.e., <100°C) sulfate reduction typically occurs after other electron acceptors are consumed. The most kinetically favorable mechanism by which sulfide is produced is through dissimilatory sulfate reduction by bacteria [Ledin and Pedersen, 1996]. Although environmental conditions may be highly variable, it is commonly accepted that the activity of sulfate reducing bacteria is directly responsible for the formation of sulfide minerals, particularly in marine environments and wetlands. Sulfate reducing bacteria account for ~50% of total carbon mineralization in active

marine sediments [Boschker *et al.*, 1998]. Moreover, the early formation of large stratiform sphalerite ore deposits may have been mediated by microorganisms under similar processes [Labrenz *et al.*, 2000]. Such microbial induced precipitation mechanisms are also of importance for environmental purposes [Boschker *et al.*, 1998; Cozzarelli *et al.*, 2000] as they regulate the cycling of elements such as iron and sulfur and may be essential in the remediation of mine wastes using natural/artificial wetlands. Moreover, organic contaminant degradation is strongly dependent on microbial induced iron and sulfate reduction linking sulfide biomineralization with bioremediation efforts [Cozzarelli *et al.*, 2000].

[3] Electrical measurements are sensitive to the pore fluid chemistry, the geometry of the pore space and the physical and chemical properties of the electrical double layer forming at the mineral-fluid interface [Vinegar and Waxman, 1984; Lesmes and Frye, 2001]. Microbial activity can profoundly alter these parameters and therefore information about microbial activity can potentially be inferred from electrical measurements. Laboratory and field experiments

¹Department of Earth and Environmental Sciences, Rutgers University, Newark, New Jersey, USA.

²Lawrence Berkeley National Laboratory, Berkeley, California, USA.

³Also at Department of Environmental Science, Policy and Management, University of California, Berkeley, Berkeley, California, USA.

illustrate that microbial hydrocarbon degradation resulted in elevated electrical conductivity [Sauck, 2000; Werkema et al., 2003]. This increase in conductivity was primarily attributed to the etching and dissolution of the mineral surface by organic acids generated during the microbial breakdown of hydrocarbons. Abdel Aal et al. [2004] showed that microbial hydrocarbon degradation in soil columns increased the electrolyte conductivity and the polarization of the soil. The enhanced polarization was attributed to microbial cell growth and biofilm formation. Naudet et al. [2003] illustrated that the redox potential distribution of a hydrocarbon plume undergoing microbial degradation is resolvable from self potential (SP) measurements. They invoked a geobattery model, whereby biofilms act as electronic conductors, to explain the SP anomaly at the leading edge of microbial zones.

[4] Our experiment considers the use of electrical measurements to observe a biomineralization process that causes mineral precipitation and mineralogical alteration. We report here electrical measurements on a column experiment loosely based on the work of Labrenz et al. [2000] and Druschel et al. [2002] and designed to represent a means of groundwater metals remediation, whereby coupled geochemical and microbial processes strip Zn and Fe from solution and precipitate metal sulfides. Our results demonstrate the potential to indirectly monitor microbial-hosted metal sulfide precipitation and show sensitivity to the distribution of the microbial population, rates of microbial activity and geometry of the resulting biomineralization. We ultimately envisage indirect electrical monitoring of the microbial remediation of heavy metals such as cadmium, lead, zinc and uranium.

2. Electrical Properties

[5] The complex conductivity (σ^*) of a soil containing metallic minerals, in the frequencies below 1 kHz, is dependent (1) on the electrolytic conductivity (σ_{el}) of the fluid in the interconnected fluid-filled pores, (2) on electronic conduction (σ_{elc}) due to the presence of metallic minerals, and (3) on the interfacial conductivity (σ_{int}^*) which is a complex term that accounts for the polarization and conduction occurring at interfaces. The σ_{el} is strongly dependent on the electrolyte conductivity (σ_w) and given by $\sigma_{el} = \sigma_w/F$, where F is a formation factor [Archie, 1942].

[6] The σ_{int}^* represents electrical double layer (EDL) conduction and polarization mechanisms that occur at interfaces, such as: (1) the non-metallic mineral-fluid interface, (2) the microbial cell-fluid interface, and (3) the metallic mineral-fluid interface. Mechanism 2 is potentially important as the ion selectivity of the outer cellular membrane of live bacterial cells in solution can generate a large low frequency polarization [Prodan et al., 2004]. Metallic minerals in solution generate a σ_{int}^* mechanism associated with the metallic mineral-fluid interface. Redox active and redox inactive ions in the EDL move predominantly perpendicular to the metal surface under application of an electric field [Wong, 1979]. This generates a diffusive mechanism (σ_{mdiff}^*) that linearly increases with the total metallic surface area in the soil [Slater et al., 2005]. Redox active ions may also generate an additional electrochemical mechanism (σ_{melc}^*) allowing electrical current to bridge the

energy barrier between electrolytic (σ_{el}) and electronic (σ_{elc}) conduction in the metal [Wong, 1979].

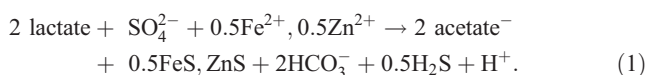
[7] The significance of the electrochemical contribution explicitly associated with the active ions is somewhat uncertain. On one hand, the active ion concentration is typically small compared with the inactive ion concentration. However, such electron shuttles can be very effective at low concentrations [Schippers and Jorgensen, 2001] and band gap bridging to lessen the energy gap in electron transfer steps may catalyze the transfer [Schoonen et al., 1998]. The relative contributions of σ_{melc}^* and σ_{mdiff}^* will critically depend on the geometric arrangement of metals in solution. Metal particles of small size that are well dispersed within a medium will have large surface area in contact with fluid, high σ_{mdiff}^* but small σ_{melc}^* as σ_{elc} is negligible. However, the same concentration of particles coagulated into a continuous metallic mineral vein will have a small surface area in contact with fluid reducing σ_{mdiff}^* but potentially increasing σ_{melc}^* by enhancing electronic conduction (σ_{elc}) through the soil. Furthermore, the dc electrical conductivity of metallic mineral deposits (due to band gap differences between minerals) varies over several orders of magnitude with mineralogy [Telford et al., 1990], thus implying that electrical measurements might also discriminate between mineral phases. In fact, the mineralogical discrimination of ore deposits with electrical measurements was treated by Pelton et al. [1978], although their results were inconclusive.

[8] The size of the metallic minerals also affects the electrical response as the polarization intensity is maximum at frequencies close to the reciprocal of the dominant relaxation time (τ) of the ions in the EDL that are polarized by the applied electric field; τ can be calculated assuming polarization of spherical grains and knowing the surface ionic diffusion coefficient. The diffusion coefficient is difficult to measure directly in porous media but it is found that τ is proportional to the square of radius of spherical grains [Schwarz, 1962]. On the basis of the existing literature [Pelton et al., 1978; Wong, 1979] we anticipate that our instrumentation is most sensitive to metallic grains above 0.001 mm radius as, below this size, the dominant relaxation occurs well above the frequency range (defined below) of our measurements [Pelton et al., 1978]. Owing to the relatively low frequency measurements employed we do not anticipate our measurements to have any significant sensitivity to nanoparticulate metal sulfides.

3. Experimental Methods

3.1. Column Setup and Sterilization

[9] The experiment involved the precipitation of iron and zinc sulfides due to microbial action under anaerobic conditions according to



The experiment was conducted entirely within an anaerobic chamber with a $\text{N}_2:\text{H}_2$ (95:5) atmosphere. Three columns were fabricated; one for electrical measurements, one for geochemical sampling and a third non-inoculated control.

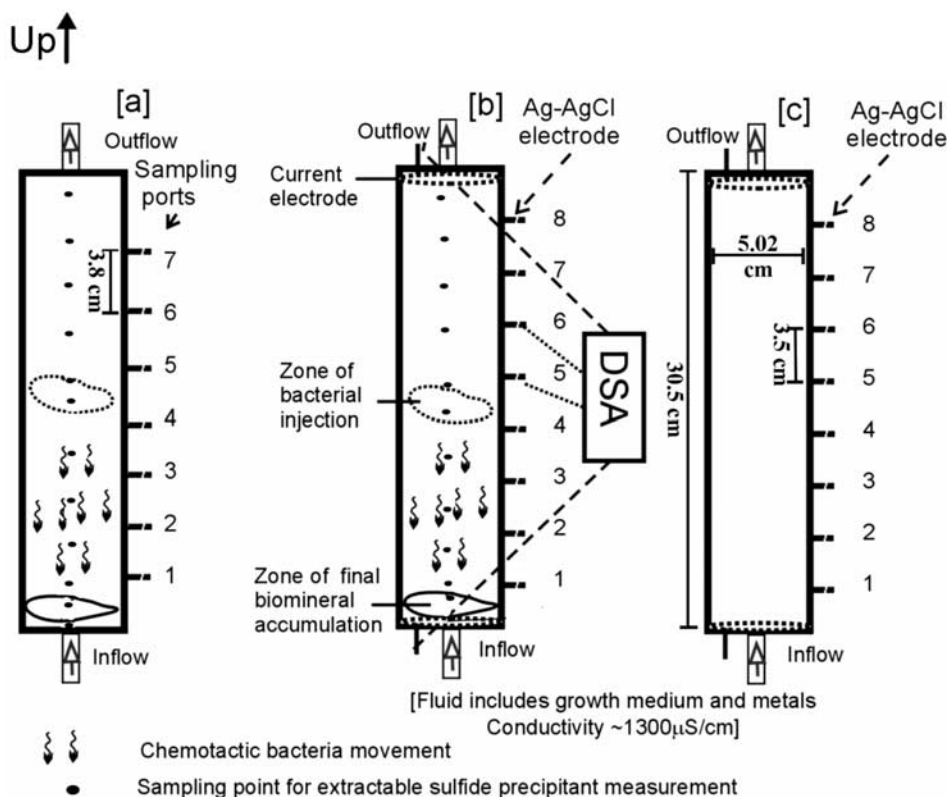


Figure 1. Schematic of experimental columns showing electrode locations, sampling points, fluid inflow, fluid outflow, zone of bacterial injection, zone of final biomineral accumulation, direction of chemotactic bacterial movement, and sample locations (center of column at 4 or 2 cm interval) for destructive analyses in (a) geochemical column, (b) electrical column, and (c) control column. Connection of the dynamic signal analyzer (DSA) to the electrical column is shown for a measurement between electrodes 5 and 6 as an example.

As the geochemical sampling ports extend to the middle of the column and could distort current flow, electrical and geochemical measurements were performed in separate identical columns to preserve minimal distortion in the electrical column (Figure 1). Each column was 30.5 cm in length with a 5.08 cm diameter. The geochemical column contained seven sampling ports at 3.8 cm separation starting from the column base. Sampling ports on the geochemical column coincided with the center of each electrode pair on the electrical column. The electrical column consisted of eight non-polarizing Ag-AgCl electrodes, which were placed 3.5 cm apart in chambers fitted onto the edge of the sample holder, in electrical contact with the soil matrix but not extending into it, in order to minimize spurious polarization that can develop at the electrode surface [Vinegar and Waxman, 1984; Vanhala and Soininen, 1995].

[10] Columns were packed with 20–30 mesh silica sand (Ottawa, IL) composed of 99.8% quartz and 0.2% magnetite with grain size varying from 600 μm up to 800 μm . Prior to packing, sand was first treated with a 6% solution of H_2O_2 to remove organics. A mixture of sodium citrate ($\text{C}_6\text{H}_8\text{O}_7\text{Na}_3 \cdot 2\text{H}_2\text{O}$), sodium bicarbonate (NaHCO_3) and sodium hydro-sulfite ($\text{Na}_2\text{S}_2\text{O}_4$) was then used to remove iron oxides. Finally, the sand was washed with deionized water, autoclaved and dried at 105°C. Columns were sterilized with ethylene oxide in a gas sterilizer and then filled with sand; the filling procedure was interrupted four times to pack the

sand by tapping the column 15–20 times. Efforts were made to pack the columns in a near identical manner; as geochemical data (discussed later) show, the columns behaved very similarly. Columns were then flushed with N_2 to remove oxygen present in the system and subsequently flushed with a de-aired growth medium composed of 2.8 mM lactate, 3.93 mM sulfate, 0.306 mM Zn^{2+} and 0.36 mM Fe^{2+} ; the growth medium was de-aired by boiling and subsequent cooling under N_2 stream and sterilized at 121°C for 15 min. Inflow was controlled by a peristaltic pump, and flow was induced from the base of the column at a velocity of 0.53 m/d. The conductivity of inflow fluid (σ_w) was 0.1300 S/m (± 0.004 S/m).

[11] The bacterium chosen for the experiment was *Desulfovibrio vulgaris* (*D. vulgaris*), a common soil and aquifer microorganism that the U.S. Department of Energy is currently investigating for its use in facilitating bioremediation in acid mine and industrial wastes. All medium components were autoclaved and cooled under continuous N_2 flow, in order to become anoxic and to remove any air. *D. vulgaris* was grown anaerobically to mid log phase in defined Widdel-Pfennig (WP) medium [Widdel and Bak, 1992]; cells were harvested by centrifugation (5000 g, 10 min, 5°C), washed twice in sterile 50-mM phosphate buffer (5.62g $\text{K}_2\text{HPO}_4/\text{L}$ and 2.13g $\text{KH}_2\text{PO}_4/\text{L}$, pH 7.0) and re-suspended in a lactate-depleted version of the minimal medium used in the experiment. The columns were inoculated by transferring aliquots

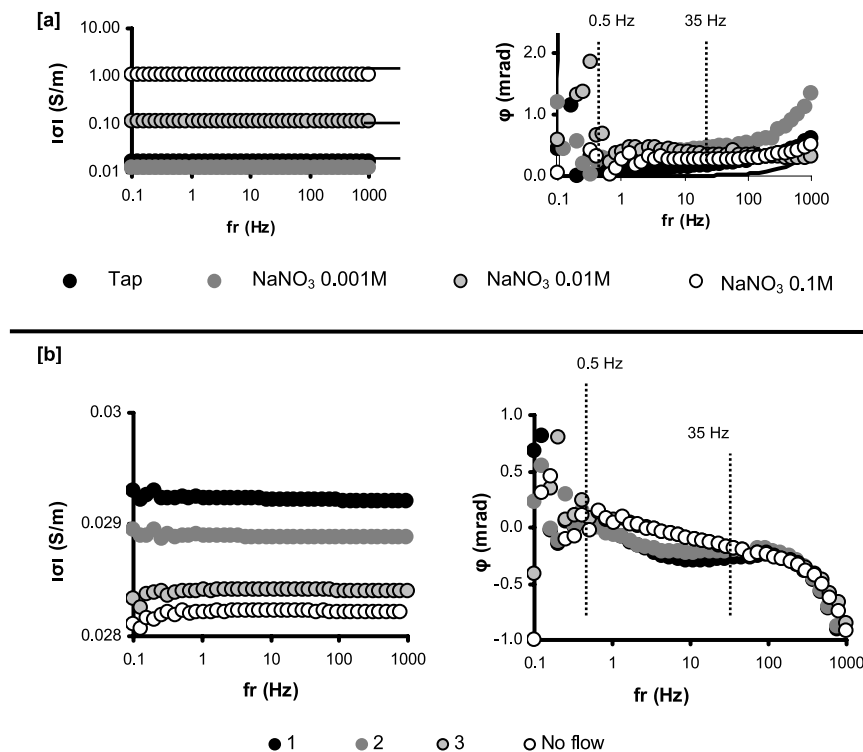


Figure 2. (a) Conductivity magnitude ($|\sigma|$) and phase (φ) measured from frequencies (fr) 01–1000 Hz for four water samples (tap water and NaNO_3 at 0.001 M, 0.01 M, and 0.1 M concentration). In each case the theoretical φ is <0.1 mrad below 100 Hz. The solid line on the φ diagram shows theoretical φ calculated for 0.001 M NaNO_3 . Phase errors are less than 0.4 mrad between 0.5 Hz and 100 Hz and are independent of sample $|\sigma|$ over three orders of magnitude (0.01–1 S/m). Between 0.1 and 0.5 Hz, the φ error increases to a maximum of 1.2 mrad. Above 100 Hz, the φ errors increase (maximum 1.4 mrad). At the higher frequency, the phase errors are greater for less conductive samples, owing to capacitive effects in the connecting wires. (b) Three repeat measurements of ($|\sigma|$) and phase (φ) acquired from the sand-filled electrical experimental column prior to bacteria injection. A maximum 3% change in $|\sigma|$ is attributed to variations in the conductivity of the saturated growth medium. Switching from no flow to flow conditions generates less than 1% change in $|\sigma|$. Above 0.5 Hz any variation in φ is less than 0.2 mrad in all cases.

of actively growing *D. vulgaris* cells with nitrogen flushed sterile syringe and injected through the top end of the columns, with the injection point close to the middle of the columns (i.e., between electrodes 4 and 5 in the electrical column and between sampling ports 4 and 5 in the geochemical column as is illustrated in Figure 1).

[12] We are confident that contamination was minimal using the sterilization procedure described above. Analysis of phospholipid fatty-acid profiles (data not shown for brevity) revealed patterns consistent with a monocultural microbial distribution along the length of the column. In addition, it is worth noting that the stimulation of sulfate-reducing microorganisms is an effective means of minimizing the impact of other potentially contaminating microflora as a result of the toxic effects of the sulfide generated as a byproduct of respiration. Finally, results from the control column, having received the identical sterilization treatment, suggest that the method was effective (data not shown for brevity).

3.2. Electrical and Geochemical Measurements

[13] Electrical measurements were made with a two-channel dynamic signal analyzer (DSA). The impedance

magnitude $|\sigma|$ and phase angle (φ) of the sample were measured relative to a resistor at 40 frequency intervals between 0.1 and 1000 Hz. Current was injected into the samples through inert gold electrodes located at both ends of the column. The measured real (σ') and imaginary (σ'') conductivity values were calculated from $|\sigma|$ and φ measurements. The real part describes conduction loss in the system, being a function of the electrolytic conduction through the pore space, the surface conduction and finally of the electronic conduction due to the presence of metals; the imaginary part describes the polarization that occurs exclusively at the interfaces (below 1000 Hz).

[14] Below 1000 Hz, $\sigma' \gg \sigma''$ and phase angles ($\varphi = \tan^{-1} \sigma''/\sigma'$) are typically less than 50 mrad. Measurements errors with our instrumentation depend on frequency. Figure 2a shows test measurements on water samples compared with calculated theoretical values (see caption for details). Between 0.5 and 100 Hz, measurement errors are generally less than 0.5 mrad for the phase and 0.5% for conductivity magnitude respectively [Slater and Lesmes, 2002a]. Additional tests were also performed to verify that the electrical measurements were not adversely affected by the establishment of fluid flow within the column. Figure 2b

shows three repeat measurements that were performed on the electrical sand-packed columns during flow and subject to a maximum 3% variation in inflow σ_w , as well as a measurement made with the flow paused (see caption for details). Above 0.5 Hz the impact of the variation in σ_w on φ is negligible whereas the difference between flow and no flow conditions is a maximum of 0.2 mrad.

[15] Geochemical sampling included analysis of sulfate, acetate, lactate, zinc and iron in solution. Fluid samples from the geochemical sampling ports as well as from the influent and effluent of all three columns were obtained. During the initial 3 weeks of the experiment geochemical sampling and electrical measurements were performed at least bi-weekly (for both experimental columns, Figures 1a and 1b), this being the maximum practical sampling rate given the time required to perform the measurements and maintain the columns. The sampling rate was reduced thereafter. This sampling scheme enabled us to detect all significant changes that were induced during the period of high microbial activity (initial 3 weeks of the experiment) and provided us with monitoring data as the column approached a steady state at later time. We will later show that chemotactic movement of *D. vulgaris* toward the base of the column occurred during the first 3 weeks and that further microbiological changes in the column were restricted to the basal few centimeters of the column closest to the nutrient inflow. A reduced sampling rate after 3 weeks was therefore justified; it was considered unlikely to temporally alias the results or miss significant microbial activity in the region above the column base. Electrical measurements and geochemical sampling were performed within 24 hours of each other (day 70 was the last day of electrical and geochemical monitoring). Sulfate, lactate, and acetate concentrations were measured using ion chromatography, and Fe and Zn concentration determined from Ion Coupled Plasma Atomic Emission Spectroscopy (ICP-AES).

[16] Following completion of geochemical and geophysical monitoring an identical flow regime was maintained for an additional 8 days until laboratory instrumentation was available for solid phase analysis. Destructive sampling of the solid phase was then performed on day 78; sediment samples were collected from the center of the column, at 4-cm intervals (at 2 cm for areas with high electrical responses), along the flow direction (Figure 1). In an effort to better preserve the grain orientations, samples were prepared for scanning electron microscopy (SEM) analysis in a manner similar to that described by *Vandevivere and Baveye* [1992]. Small cylinders (0.5 × 1 cm) were inserted into the column sediments at 4-cm intervals, removed and capped with fine mesh. The capped cylinders were immersed overnight in a 2.5% solution of glutaraldehyde, rinsed 3 times in phosphate buffer, dehydrated in an ethanol series, and dried in a critical point drying unit with CO₂ as the transitional fluid. The sediments were then extruded from the cylinders onto carbon-coated SEM stubs and immediately analyzed using a Philips XL30 scanning electron microscope (SEM) fitted with backscatter and secondary electron detectors and an energy dispersive X-ray (EDX) analytical system. The backscattered electron data were used to isolate electron dense (i.e., metal rich) regions along the sediment surfaces and the EDX was used to map the constitutive elements in the regions. SEM was also used

to assess sediment affixed cell densities, permit mineral identification and to investigate the spatial relationship between sulfide precipitates and microbes. ICP-AES was utilized to determine the distribution of solid phase Zn and Fe on sand grains by dissolution of 1 g sample in 6 M HCl. This method was considered appropriate to meet the objectives in this study (correlation of regions of biomineralization with electrical measurements) as formation of pyrite was deemed unlikely under our experimental conditions [Benning *et al.*, 2000].

[17] A second experiment was performed whereby the biogeochemical conditions were replicated, except that the metals were excluded from the flow medium; the second experiment was a complete repeat of the first experiment, using the same columns, replacing all disposable materials and using fresh sand matrix and fluids all treated and prepared exactly in the same way as the first experiment but excluding the metals. In this experiment we focused primarily on electrical measurements as a full geochemical analysis of this simpler system was beyond the scope of our objective, being to isolate any effect on the electrical measurements of the microbial cells themselves from the electrical signature of metal precipitates formed during microbial sulfate respiration.

4. Results

4.1. Biogeochemical Results

[18] Geochemical analysis of the effluent of both the geochemical and electrical columns as a function of time shows that the columns behaved very similarly (break-through curves shown in Figure 3). We therefore assume that (1) similar biogeochemical processes occurred in both columns and (2) direct comparison of the electrical and geochemical measurements is valid. These results also verify that mineral precipitation proceeded roughly according to stoichiometric calculations (equation (1)); sulfate and lactate concentrations, as well as metals in solution, decrease as expected, indicating that mineralization occurs as a result of biogeochemical activity. Note that sulfate reaches a pseudo state concentration 15–20 days later than lactate and then fluctuates around the lowest concentration (fluctuation is minimal, close to instrument accuracy); this behavior is probably attributed to the fact that after lactate is depleted (limiting factor), hydrogen, produced by the microbial biomass fermentation, is used as a reductant to maintain growth as our system is not sulfate limited; as a result sulfate reduction (non-stoichiometric) continues after lactate depletion. Microbial biomass (data not shown for brevity) supports this argument as viable biomass is observed at distances downgradient of the region of lactate depletion.

[19] SEM analysis showed that the metal-rich regions consisted of a roughly 1:1 ratio of zinc, iron and sulfur and, most significantly, confirmed that the sulfide precipitation was associated with cellular surfaces. Figure 4a is an SEM image of a single bacterial cell with metal sulfide nodules coating the outer membrane of the bacterium. This sample was recovered from sediments 25 cm from the influent end upon termination of the experiment. It is important to note that the bacterium appears viable; the presence of a flagellum suggests that this microbe is still

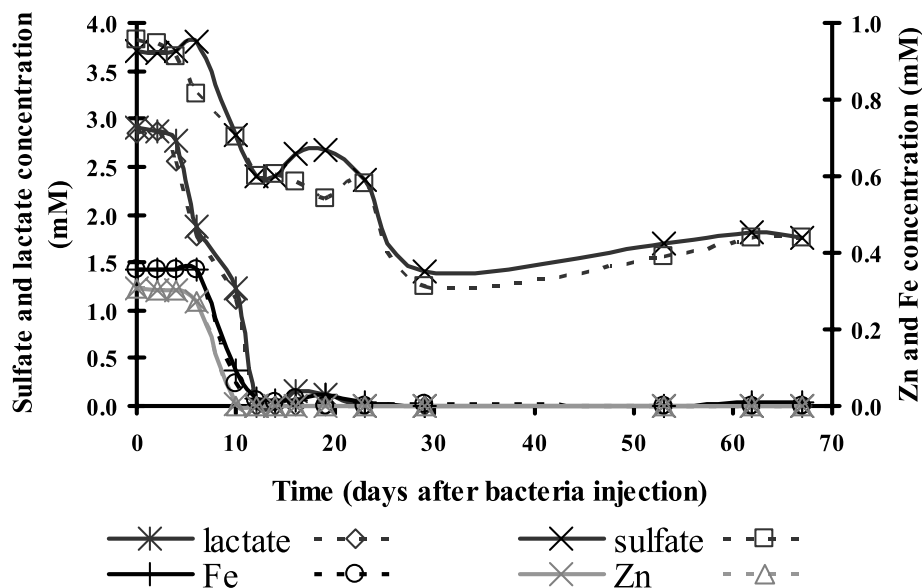


Figure 3. Breakthrough curves of the outflow geochemistry of electrical (open symbols with dashed line) and geochemical (symbols with solid line) columns indicating that similar biogeochemical reactions occurred (or “conditions existed over time”) in each column.

motile even with the sulfide coating (for brevity these viable metal sulfide encrusted cells will be referred to as “biominerals”). Figure 4b shows thick, mineralized cell deposits (biofilms) located on quartz grains (referred to as “mineralized biofilms” hereafter, for brevity); this sample was extracted from sediments located within the first 2 cm from the inflow end of the column upon completion of the experiment. The detailed destructive analysis (sampling locations illustrated in Figure 1) revealed that microbial biomass throughout and within the column increases toward the base of the column where 83% of the extractable iron and 93% of the extractable zinc are located (Figure 5). Slightly elevated concentrations of extractable metals within the column also occur in the vicinity of bacterial injection

between electrodes 4 and 5 (Figure 5). In order to identify the chemical composition of the metal rich areas we used the backscattered electron data to isolate electron dense regions along the sediment surfaces; following the isolation of such regions, we used the EDX information to map the constitutive elements, and in all instances, we found the metal-rich regions to consist of roughly 1:1 ratios of zinc, iron and sulfur (data not shown).

[20] A narrow black colored band of precipitation indicative of FeS was observed to form along the inside edge of the column starting between electrode pairs 4 and 5 and widening toward the column base with time. Development of this precipitant band coincided with the depletion of the metals in solution although it did not represent a signifi-

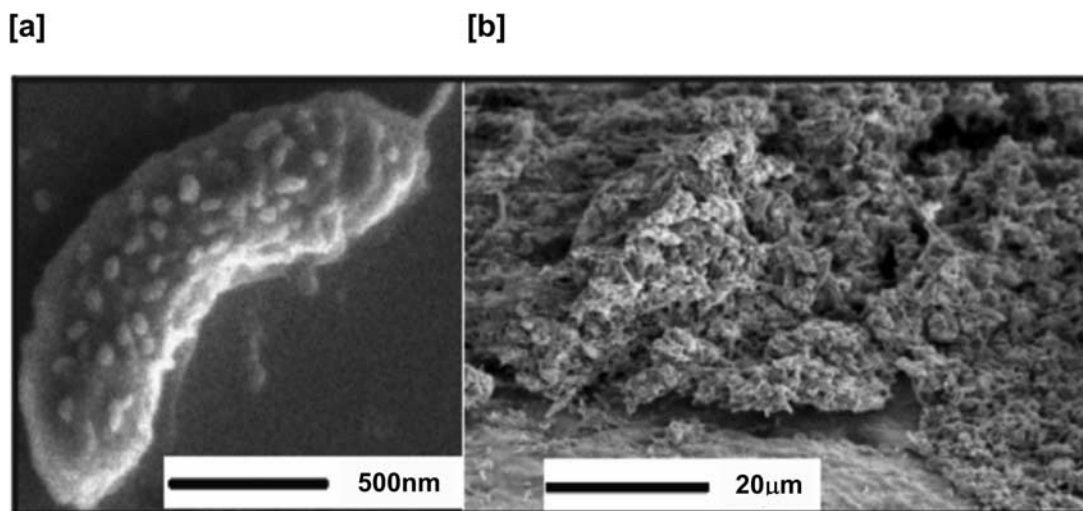


Figure 4. Scanning electron microscope (SEM) images of samples obtained from two locations within the inoculated, metals-amended electrical column after 78 days. (a) Biomineral (25 cm from influent end of column), and (b) quartz grain encrusted with a mineralized biofilm (2 cm from influent end).

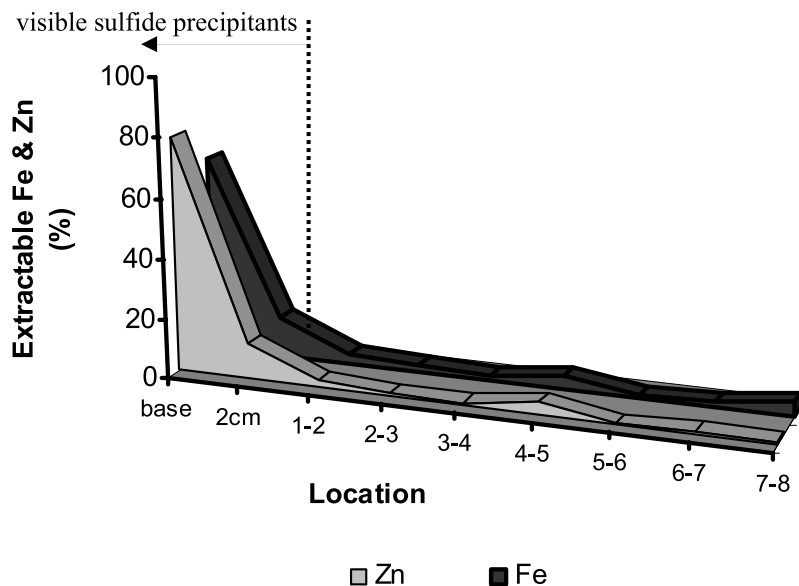


Figure 5. Total extractable Zn and Fe as a function of distance from the influent end at termination of experiment after 78 days; ~80% of the extractable metal is within 2 cm of the base (modified from data presented by Williams *et al.* [2005]).

cant proportion of the metals extracted from the column (Figure 5). The lowest 2–3 cm of the column eventually turned completely black, indicating extensive FeS precipitation in this region. White precipitates, indicative of the formation of ZnS were not observed at any location or time in the column. The overall distribution of extractable metals and the mineralized biofilms results from the chemotactic movement (movement of an organism toward a chemical gradient) of *D. vulgaris* toward the column base. The spatial distribution of mineral precipitates and biominerals was similar in the two inoculated columns. Further details on the biogeochemical performance of the system and detailed discussion are given by Williams *et al.* [2005].

[21] As the second (no metals) experiment was designed solely to contrast the electrical response of the same system when metals were excluded, a detailed biogeochemical analysis of this experiment is excluded for brevity. The sulfate and lactate concentrations as a function of time and location closely parallel those already presented for the first experiment (Figure 3). Mass balance calculations using the ICP data from this second experiment suggested that acid metal extractions were unnecessary.

4.2. Electrical Results

[22] Figures 6a and 6b show measured σ' (conduction) and σ'' (polarization) values at 35 Hz between electrode pairs 1–2, 3–4, 4–5 and 6–7 over the experiment duration with metals in solution. Although the electrical data show some frequency dependence the primary characteristics of the data set are reproduced at any frequency between 1 and 100 Hz as observed in Figure 6c where representative spectral data from electrode pair 4–5 for selected days are plotted; σ'' shows changes between 0.5 and 500 Hz, being pronounced between 1 and 100 Hz; σ' appears relatively stable for the same dates and frequency range. The 35-Hz data focus on the area where polarization is most pronounced and show the lowest error in phase shift

(Figure 2). Results for electrode pairs 5–6 and 7–8 (above the zone of injection and outside of the region of chemotactic cell movement) are not shown, but are consistent with those obtained between 6 and 7. Similarly, the results on pair 2–3 are almost identical to those obtained on pair 3–4, both pairs being between the zone of injection and the zone of biomineral accumulation (Figure 1).

[23] We observe that (1) changes in σ'' are greater than changes in σ' ; (2) the electrode pair centered at the bacterial injection location (4–5) and the electrode pair closest to the final microbial accumulation (1–2) show the largest temporal changes in σ'' . At the zone of bacterial injection (4–5), we observe an increase in σ'' after 4 days with a σ'' peak on day 10. The σ'' then recedes from day 12 to the end of the experiment, reaching pre-injection values by day 48. A similar temporal response is recorded for pairs 1–2 (just above the zone of final bacterial accumulation). However, this σ'' response near the nutrient inlet differs from that at the bacterial injection location in that: (1) the maximum σ'' is greater; (2) the onset of the σ'' increase occurs approximately 7 days later, and (c) the recession of the σ'' anomaly is initially steeper, reaching a minimum at day 48, recovering very slightly by day 70 yet remaining above pre-injection levels throughout the duration of the experiment. The significance of the slight increase after day 48, based on only one point, is uncertain but could reflect further biogeochemical system change. Figure 6d shows representative spectral σ'' measurements acquired from the control column before (day 3) and during the period of observed changes in the electrical column (days 4 and 13).

[24] Figure 6a shows that the real conductivity (σ') recorded on electrode pair 1–2 (just above the zone of final bacterial accumulation) fluctuates between 0.028 and 0.03 S/m until day 12 (time of σ'' peak) but then exhibits a clear, consistent increase with time until the end of the experiment. This σ' increase coincides with a decrease in

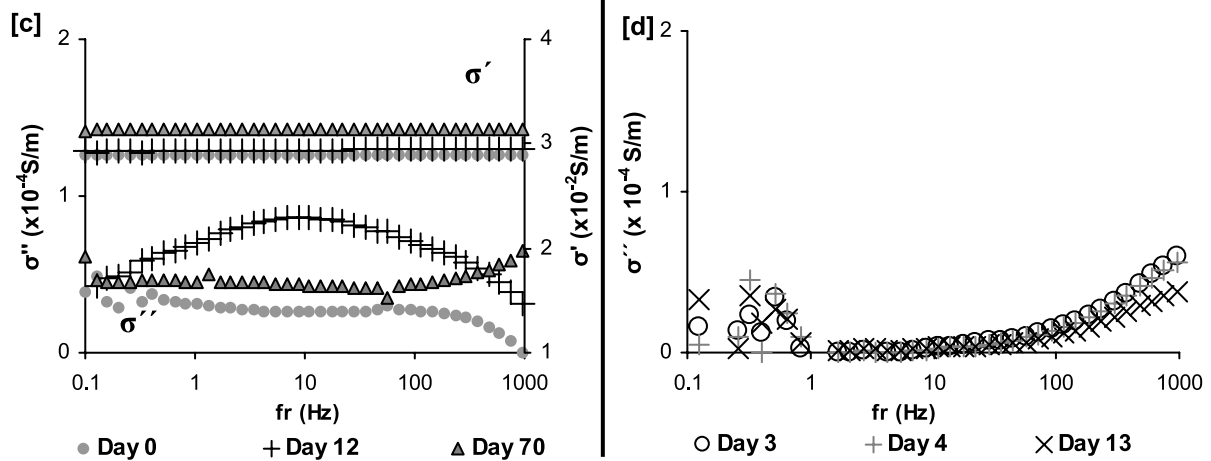
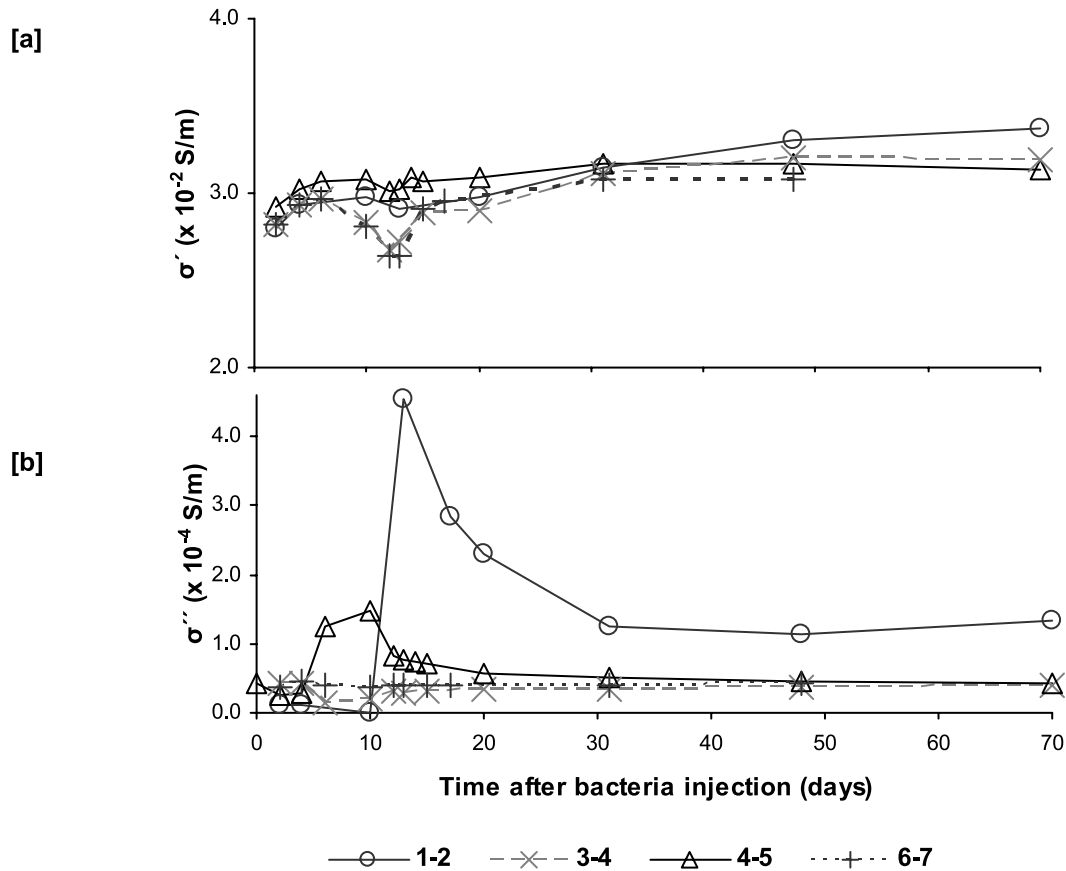


Figure 6. (a) Real conductivity (σ') and (b) imaginary conductivity (σ'') as a function of time between electrode pairs 1–2, 3–4, 4–5, and 6–7 at 35 Hz for the experiment run with metals; the last data set of electrode pair 6–7 is omitted due to an instrumentation error; (c) representative real (σ') and imaginary (σ'') conductivity spectra from frequencies (fr) 0.1–1000 Hz for selected days from electrode pair 4–5; and (d) control column response at selected times after injection.

σ'' . At all other locations in the column there is no systematic change in σ' . The irregular behavior of σ' during the first 12 days of the experiment (most apparent for electrode pairs 3–4 and 6–7) may reflect slight changes in σ_w of the circulating fluid as observed in control experiments. However, the magnitude of these early changes does not exceed the magnitude of the σ' changes observed in the control column.

[25] Figure 7 compares the variation in σ'' at electrode pairs 1–2 and 4–5 for the experiment conducted in the column where metals were excluded (NM) with measurements recorded from the columns that had metals in solution (M), as detailed above and previously shown in Figure 6a. The σ'' at 4–5 (NM) is comparable to that for sediment extracted at the top of the column where no precipitation occurred (0.1×10^{-4} S/m) and indicative of negligible

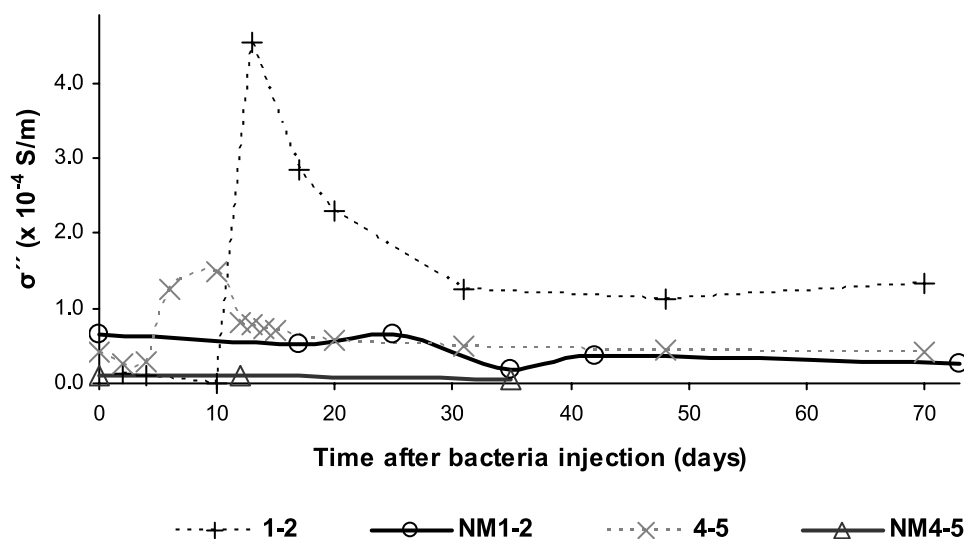


Figure 7. Imaginary conductivity (σ'') response (35 Hz) obtained for the experiment run without metals (the response recorded with metals (Figure 6a) is superimposed for direct comparison). Note here that the σ'' magnitude recorded for a heavily sulfide encrusted sediment (active biomineralization) sample extracted from the column base was 5.5×10^{-4} S/m; similarly, for sediment extracted at the top of the column where no precipitation occurred the σ'' magnitude recorded was 0.1×10^{-4} S/m.; NM 4–5 was terminated at day 35 as no significant changes were recorded at 4–5 (metals experiment) after this time.

polarization. At electrode pair 1–2 (NM), immediately above the zone of final bacterial accumulation, σ'' is somewhat greater than at 4–5 (NM) but is small and devoid of characteristic temporal behavior when compared to the response obtained at pair 1–2 (M). Figure 7 also shows σ'' (5.5×10^{-4} S/m) for a heavily sulfide encrusted sand sample extracted from the very base of the column on day 78, where mineralized biofilms accumulated (Figure 4).

5. Discussion

[26] Microbial lactate and sulfate consumption in the metals experiment led to acetate production, precipitation of metals from solution in the form of insoluble iron and zinc sulfide minerals, following equation (1). These reactions were confirmed by geochemical monitoring, visual evidence of metal sulfide formation (appearing as a black precipitant mostly at the base of the microbial active metal column), and SEM imaging/chemical analysis. Iron and zinc sulfides precipitated onto bacterial cells forming a metallic coating on the outer cell wall, or a “biomineral.” Following an initial lag phase, subsequent microbial growth coincided with chemotactic movement toward the base of the column, the region having the greatest nutrient concentration. This ultimately constrained the accumulation of biominerals and, later, mineralized biofilms formed at the base of the column within the area of active sulfate reduction (Figure 5). Geochemical data, presented as breakthrough curves for lactate, sulfate, Zn and Fe in solution, (Figure 3) show that both inoculated columns (electrical and geochemical) behaved very similarly, permitting the direct comparison and interpretation of the electrical data in terms of the biogeochemical evolution of the columns.

[27] We first consider the mechanism generating the polarization (σ'') anomalies observed during the experiment

(Figures 6 and 7). We previously suggested polarization mechanisms associated with the microbial cell-fluid interface and the metallic mineral precipitate-fluid interface; we neglect polarization at the non-metallic mineral-fluid interface as it is negligible in the quartz sand used for this experiment. Comparison of experimental results with and without metals (all other system parameters equal), suggests that the polarization anomaly is primarily associated with the metallic mineral precipitate-fluid interface that exists as a result of metal sulfide formation. Polarization measured on the experiment without metals is minimal (Figure 7). We therefore suggest that the polarization increase is associated with the increase of polarizable particles (biominerals) accompanying microbial metabolism and growth. Measurements on sulfide-encrusted (bottom of column) and sulfide-free sand grains (top of column) extracted upon termination of the experiment support this argument. The sulfide-encrusted sand grains exhibit a large σ'' (5.5×10^{-4} S/m at 35 Hz) while the “clean” sands show σ'' comparable to the control column (0.1×10^{-4} S/m at 35 Hz) as well as the active “metal free” column (Figure 7).

[28] We next consider the timing of the σ'' anomalies observed in the columns containing metals. Following inoculation and phase lag (4 days), polarization increased at the injection area (electrode pair 4–5, Figure 6). A larger σ'' increase later occurred toward the column base (electrode pair 1–2, Figure 6), where biominerals finally accumulated owing to chemotaxis. No significant response was observed between the zones of injection and final accumulation (electrode pairs 2–3 and 3–4) as well as above the injection area (above electrode pair 4–5). This response is consistent with the characteristics of microbial cell metabolism and chemotactic movement. We attribute the lag between bacterial injection and onset of polarization at the injection location to the time required for the microbial population to equilibrate to its new, nutrient enriched environment.

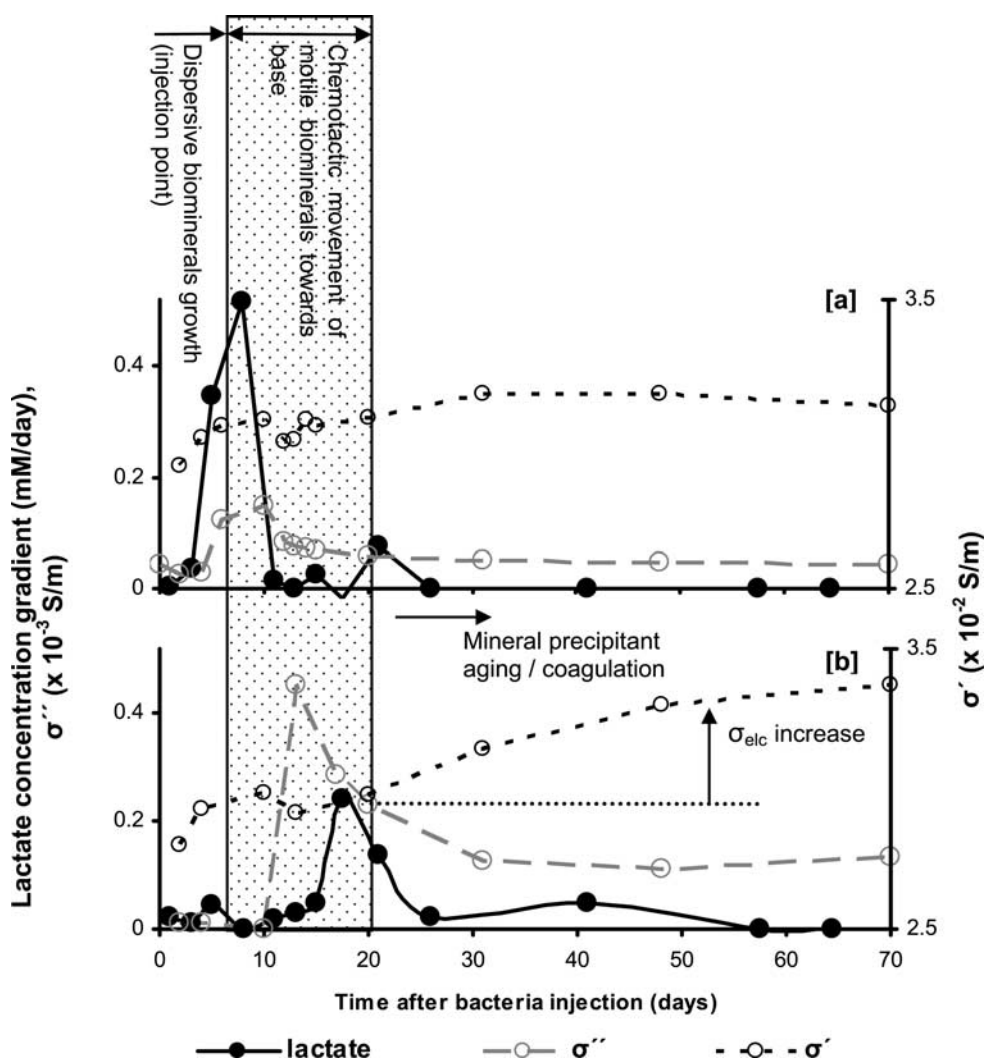


Figure 8. Gradient of lactate concentration (calculated from breakthrough curve of lactate in Figure 3) over time at the zones of (a) microbial injection (sampling port 5) and imaginary (σ'') and real conductivity (σ') observed at electrode pair 4–5 (injection); and (b) final biomineral accumulation (sampling port 1) in the geochemical column and imaginary (σ'') and real conductivity (σ') observed at electrode pair 1–2 (final accumulation). Interpreted biomineral growth, movement, and mineralization stages also shown. The measurements are from the first experiment with metals.

Microbial metabolism initially occurs in the region of the injection, generating polarizable biominerals. The pseudo steady state nutrient concentration gradient then drives the microbial community toward the nutrient inflow. This occurs as a gradual (rather than bulk) transfer of microbial mass from the center to the bottom of the column. We assume that the concentration of biominerals involved in chemotactic movement from the injection zone toward the nutrient inflow at any one time was insufficient to cause a detectable polarization response, i.e., the concentration of biominerals between the injection and accumulation zones remained at or below the detection limit of our instrument (detectable concentrations only existed at the injection point and final accumulation point, these being the areas with the highest extractable metal concentration). The cumulative arrival and accumulation of biominerals at the column base later causes the large σ'' response observed.

[29] Figure 8 shows the gradient of the lactate concentration for the experiment with metals (calculated from the breakthrough curve in Figure 3 as the difference in concentration divided by the time elapsed between consecutive measurements) at the zone of microbial injection (electrode pair 4–5) and at electrode pair 1–2 closest to the zone of final accumulation. This gradient is indicative of the average rates of microbial metabolism and cell respiration at the two locations. We assume that high metabolic rates result from high cell concentrations, high sulfate respiration and high concentrations of biominerals. The σ'' observed at these two zones is re-plotted in Figure 8 for comparison. We attribute the similar timing of the peaks in σ'' and the calculated lactate concentration gradient to a surface area effect: The peak in microbial activity correlates with maximum concentration of dispersed biominerals, maximum metal-fluid interfacial surface area and hence maximum σ'' . The onset of polarization increase correlates well with

the onset of lactate consumption (microbial metabolism) at both locations in the column (about 4 days at pair 4–5 and 10 days at pair 1–2).

[30] We next consider the significance of the decrease in σ'' following the peak in metabolism inferred from the lactate concentration gradient (Figure 8). At the injection location (4–5), σ'' approaches pre-injection values by day 48. We attribute this to the eventual chemotactic migration of all biominerals away from this region such that any remaining are below the detection limits of our instrument. More complex is the reduction in σ'' near the base of the column (1–2) where permanent sulfide precipitates were visibly observed to form by day 31. At this location σ'' reduces after day 13 but never returns to pre-injection values. SEM images indicate differences in the crystal structure, deposition and geometry of the sulfide precipitates with time as apparent in Figure 4. These images represent the different stages of biomineralization process. At early stages of biomineralization, sulfide precipitates are dispersed on motile cells (Figure 4a), such that the microbial community exhibits a high mineral-fluid interfacial surface area. At later times, the sulfide precipitates are compacted forming biofilms on grain surfaces (Figure 4b) resulting in reduced mineral-fluid interfacial surface area. Note that at later times, the total surface area of the mineral precipitate may actually be higher than at early times but it is only the surface in contact with the pore filling fluid that contributes to the polarization; as a result of mineral clogging of the pore space this surface area will presumably decrease. We thus attribute the drop in σ'' near the column base (1–2) to result from this geometric rearrangement of polarizable biominerals coupled with any further movement of biominerals toward the very base of the column below pair 1–2. We suggest that the residual polarization associated with the final mineralized biofilms (measured to be even greater (5.5×10^{-4} S/m) in the sample extracted from the very base of the column) is partly due to an increase in σ_{mech}^* following this geometric rearrangement of minerals. This is supported by the increase in σ' at 1–2 (Figure 8b) that we attribute to significant σ_{elec} resulting from the development of compacted and continuous electronically conductive mineral biofilms throughout and within the column (Figure 4b). No significant increase in σ' occurs at the zone of injection where such mineralization is absent (Figure 8a). This interpretation of the electrical measurements is summarized in the annotations on Figure 8.

[31] Our work shows that low-frequency electrical measurements may aid in the indirect monitoring of microbial processes in the laboratory. The induced polarization (IP) method, whereby $|\sigma|$ and φ are measured using a four electrode arrangement, has been applied for locating economically viable disseminated metal sulfide deposits in the earth [Marshall and Madden, 1959; Sumner, 1976; Pelton et al., 1978; Vanhala, 1997] and is capable of resolving as low as 1% metal sulfide concentration. Recently, IP has been utilized in environmental and engineering applications [Ward et al., 1995; Lesmes and Frye, 2001; Slater and Lesmes, 2002b]. In our laboratory columns the maximum recorded φ was 14 mrad. Such relatively small IP measurements are still accurately recordable and diagnostic of detectable environmental processes [e.g., Kemna et al., 2004]. Measured phase values would increase in less

conductive media (all other factors being equal). We thus consider IP measurements a promising method for indirect investigation of microbial processes in the earth.

6. Conclusions

[32] We have measured the low-frequency electrical signature of a microbial-mediated metal sulfide precipitation process occurring in a quartz-packed sand column. Our measurements are consistent with biomineralization processes occurring in the column as determined from geochemical and destructive analyses. The electrical signature of dispersed biominerals forming at early stages is distinctly different to that of mineralized biofilms. The measured polarization detected the onset of microbial activity and was similar in temporal character to the rate of microbial metabolism inferred from rates of lactate consumption. The results indicate that the polarization appears to increase with the amount of biomineral-fluid interfacial surface area at any time; this polarization is high for well dispersed biominerals and reduces as they later cluster at the nutrient source to fill the pore space and promote electronic conduction. The magnitude of the response appears sufficient to be measured with geophysical field instrumentation. Our results imply that electrical monitoring of microbial processes involving the remediation of heavy metals (e.g., cadmium, lead, zinc, and uranium) through sequestration in insoluble precipitates is viable.

[33] **Acknowledgments.** This study was funded by the Department of Energy, Environmental Management Science Program (EMSP) grant DE-AC03-76SF00098 to S. Hubbard. Electron microscopy was performed at the DOE William R. Wiley Environmental Molecular Sciences Laboratory, with the assistance of Alice Dohnalkova and Jim Young (PNNL).

References

- Abdel Aal, G. Z. A., E. A. Atekwana, L. D. Slater, and E. A. Atekwana (2004), Effects of microbial processes on electrolytic and interfacial electrical properties of unconsolidated sediments, *Geophys. Res. Lett.*, *31*, L12505, doi:10.1029/2004GL020030.
- Archie, G. E. (1942), The electrical resistivity log as an aid in determining some reservoir characteristics, *Trans. Am. Inst. Min. Metall. Pet. Eng.*, *146*, 54–62.
- Benning, L. G., R. T. Wilkin, and H. L. Barnes (2000), Reaction pathways in the Fe-S system below 100 degrees C, *Chem. Geol.*, *167*(1-2), 25–51.
- Boschker, H. T. S., S. C. Nold, P. Wellsbury, D. Bos, W. de Graaf, R. Pel, R. J. Parkes, and T. E. Cappenberg (1998), Direct linking of microbial populations to specific biogeochemical processes by C-13-labelling of biomarkers, *Nature*, *392*(6678), 801–805.
- Cozzarelli, I. M., J. M. Sufita, G. A. Ulrich, S. H. Harris, M. A. Scholl, J. L. Schlottmann, and S. Christenson (2000), Geochemical and microbiological methods for evaluating anaerobic processes in an aquifer contaminated by landfill leachate, *Environ. Sci. Technol.*, *34*(18), 4025–4033.
- Druschel, G. K., M. Labrenz, T. Thomsen-Ebert, D. A. Fowle, and J. F. Banfield (2002), Geochemical modeling of ZnS in biofilms: An example of ore depositional processes, *Econ. Geol.*, *97*(6), 1319–1329.
- Kemna, A., A. Binley, and L. Slater (2004), Crosshole IP imaging for engineering and environmental applications, *Geophysics*, *69*(1), 97–107.
- Labrenz, M., et al. (2000), Formation of sphalerite (ZnS) deposits in natural biofilms of sulfate-reducing bacteria, *Science*, *290*(5497), 1744–1747.
- Ledin, M., and K. Pedersen (1996), The environmental impact of mine wastes—Roles of microorganisms and their significance in treatment of mine wastes, *Earth Sci. Rev.*, *41*(1–2), 67–108.
- Lesmes, D. P., and K. M. Frye (2001), Influence of pore fluid chemistry on the complex conductivity and induced polarization responses of Berea sandstone, *J. Geophys. Res.*, *106*(B3), 4079–4090.
- Marshall, D. J., and T. R. Madden (1959), Induced polarization: A study of its causes, *Geophysics*, *24*(4), 790–816.
- Naudet, V., A. Revil, J. Y. Bottero, and P. Begassat (2003), Relationship between self-potential (SP) signals and redox conditions in contaminated

- groundwater, *Geophys. Res. Lett.*, 30(21), 2091, doi:10.1029/2003GL018096.
- Pelton, W. H., L. Rijo, and C. M. Swift Jr. (1978), Inversion of two-dimensional resistivity and induced polarization data, *Geophysics*, 43(4), 788–803.
- Prodan, C., F. Mayo, J. R. Claycomb, J. H. Miller, and M. J. Benedik (2004), Low-frequency, low-field dielectric spectroscopy of living cell suspensions, *J. Appl. Phys.*, 95(7), 3754–3756.
- Sauck, W. A. (2000), A model for the resistivity structure of LNAPL plumes and their environs in sandy sediments, *J. Appl. Geophys.*, 44, 151–165.
- Schippers, A., and B. B. Jorgensen (2001), Oxidation of pyrite and iron sulfide by manganese dioxide in marine sediments, *Geochim. Cosmochim. Acta*, 65(6), 915–922.
- Schoonen, M. A. A., Y. Xu, and D. R. Strongin (1998), An introduction to geocatalysis, *J. Geochem. Explor.*, 62(1–3), 201–215.
- Schwarz, G. (1962), A theory of the low-frequency dielectric dispersion of colloidal particles in electrolyte solution, *J. Phys. Chem.*, 66, 2636–2642.
- Slater, L. D., and D. Lesmes (2002a), Electrical-hydraulic relationships observed for unconsolidated sediments, *Water Resour. Res.*, 38(10), 1213, doi:10.1029/2001WR001075.
- Slater, L. D., and D. Lesmes (2002b), IP interpretation in environmental investigations, *Geophysics*, 67(1), 77–88.
- Slater, L., J. Choi, and Y. Wu (2005), Electrical properties of iron-sand columns: Implications for induced polarization investigation and performance monitoring of iron-wall barriers, *Geophysics*, 70(4), 87–94.
- Sumner, J. S. (1976), *Principles of Induced Polarization for Geophysical Exploration*, 277 pp., Elsevier, New York.
- Telford, W., L. Geldart, and R. Sheriff (1990), *Applied Geophysics*, 2nd ed., Cambridge Univ. Press, New York.
- Vandevivere, P., and P. Baveye (1992), Sampling method for the observation of microorganisms in unconsolidated porous-media via scanning electron-microscopy, *Soil Sci.*, 153, 482–485.
- Vanhala, H. (1997), Mapping oil-contaminated sand and till with the spectral induced polarization (SIP) method, *Geophys. Prospect.*, 45, 303–326.
- Vanhala, H., and H. Soininen (1995), Laboratory technique for measurement of spectral induced polarization response of soil samples, *Geophys. Prospect.*, 43, 655–676.
- Vinegar, H. J., and M. H. Waxman (1984), Induced polarization of shaly sands, *Geophysics*, 49(8), 1267–1287.
- Ward, S. H., B. K. Sternberg, D. J. Labrecque, and M. M. Poulton (1995), Recommendations for IP research, *Leading Edge*, 14, 243–247.
- Werkema, D. D., E. A. Atekwana, A. L. Endres, W. A. Sauck, and D. P. Cassidy (2003), Investigating the geoelectrical response of hydrocarbon contamination undergoing biodegradation, *Geophys. Res. Lett.*, 30(12), 1647, doi:10.1029/2003GL017346.
- Widdel, F., and F. Bak (1992), Gram-negative mesophilic sulfate reducing bacteria, in *The Prokaryotes: A Handbook on the Biology of Bacteria—Ecophysiology, Isolation, Identification, Applications*, 2nd ed., edited by A. Balows et al., pp. 3352–3378, Springer, New York.
- Williams, K. H., D. Ntarlagiannis, L. D. Slater, A. Dohnalkova, S. S. Hubbard, and J. F. Banfield (2005), Geophysical imaging of stimulated microbial biomineralization, *Environ. Sci. Technol.*, in press.
- Wong, J. (1979), An electrochemical model of the induced-polarization phenomenon in disseminated sulfide ores, *Geophysics*, 44(7), 1245–1265.

S. Hubbard and K. H. Williams, Lawrence Berkeley National Laboratory, 1 Cyclotron Rd. MS-90-1116, Berkeley, CA 94720, USA.

D. Ntarlagiannis and L. Slater, Department of Earth and Environmental Sciences, Rutgers University, 101 Warren Street, Room 137, Newark, NJ 07102, USA. (dimntar@pegasus.rutgers.edu)